Three-dimensional Structure of the Z Band in a Normal Mammalian Skeletal Muscle

John P. Schroeter,*‡§ Jean-Pierre Bretaudiere,‡ Ronald L. Sass,§ and Margaret A. Goldstein*

*Department of Medicine, Baylor College of Medicine, Houston, Texas 77030; ‡Department of Pathology and Laboratory Medicine, University of Texas Health Science Center at Houston, Houston, Texas 77030; and §Department of Ecology and Evolutionary Biology, Rice University, Houston, Texas 77251

Abstract. The three-dimensional structure of the vertebrate skeletal muscle Z band reflects its function as the muscle component essential for tension transmission between successive sarcomeres. We have investigated this structure as well as that of the nearby I band in a normal, unstimulated mammalian skeletal muscle by tomographic three-dimensional reconstruction from electron micrograph tilt series of sectioned tissue.

The three-dimensional Z band structure consists of interdigitating axial filaments from opposite sarcomeres connected every 18 ± 12 nm (mean ± SD) to one to four cross-connecting Z-filaments. Most often, the cross-connecting Z-filaments are observed to meet the axial filaments in a fourfold symmetric arrangement. The substantial variation in the spacing between cross-connecting Z-filament to axial filament connection points suggests that the structure of the Z band is not determined solely by the arrangement of α-actinin to actin-binding sites along the axial filament. The cross-connecting filaments bind to or form a "relaxed interconnecting body" halfway between the axial filaments. This filamentous body is parallel to the Z band axial filaments and is observed to play an essential role in generating the small square lattice pattern seen in electron micrographs of unstimulated muscle cross sections. This structure is absent in cross sections of the Z band from muscles fixed in rigor or in tetanus, suggesting that the Z band lattice must undergo dynamic rearrangement concomitant with crossbridge binding in the A band.

THE Z band is an identifying feature of striated muscle. The filamentous Z band lattice defines either end of the muscle sarcomere and is essential for force transmission between sarcomeres. It is also likely that the Z band is involved in coordination of contractile and elastic forces in muscle.

At the Z band the thin filaments, which are composed primarily of actin, become linked by a dense net of cross-connecting Z-filaments of which α-actinin is an important structural component (Suzuki et al., 1976). The extensions of the thin filaments into the Z band, termed the Z band axial filaments, retain an actin core (Yamaguchi et al., 1983*a*; Zimmer and Goldstein, 1987*a*). A number of other proteins are known components of the Z band and may be portions of the axial filaments (Vigoreaux, 1994). It is also known that α-actinin coats the surface of the axial filaments in the Z band (Zimmer and Goldstein, 1987*b*). The Z band axial filaments and cross connections form an ordered, paracrystalline array as seen in electron micrographs of cross and longitudinal sections from striated muscle. An amorphous matrix material is visible in electron micrographs of the Z band and is believed to fill the spaces between the ordered filamentous components (Kelly and Cahill, 1972; Takahashi and Hattori, 1989). Although Z bands from both insect and vertebrate muscle contain actin and α-actinin as major components, the Z band paracrystal exhibits different symmetries (threefold in cross section versus fourfold) in the two muscle types (Knappeis and Carlsen, 1962; Auber and Couteaux, 1963; Ashhurst, 1967). A 3-D reconstruction of the honeybee flight muscle Z band revealed a structure of interdigitating axial filaments arranged in triplets with an overall hexagonal symmetry joined by a complex array of five different linkages (Cheng and Deatherage, 1989; Deatherage et al., 1989). A later reconstruction of the human nemaline rod, a pathologically widened Z band state associated with nemaline myopathy, revealed a much simpler lattice. The nemaline rod was found to exhibit a pseudo-fourfold screw symmetry about the axial filament axis, with a single type of connecting structure (Morris et al., 1990).

In longitudinal projections of vertebrate striated muscle (i.e., the direction of projection perpendicular to the sarcomere axis), Z bands of varying width have been ob-

Address all correspondence to Dr. John P. Schroeter, Department of Medicine, Section of Cardiovascular Sciences, Baylor College of Medicine, One Baylor Plaza, Houston, TX 77030. Tel.: (713) 798-6260. Fax: (713) 790-0681. E-mail: schroet@iris.med.uth.tmc.edu

served. The width variation seems to depend upon additional stacking of simple one-subunit Z bands in the longitudinal direction (Rowe, 1973; Goldstein et al., 1977), that is, along the sarcomere axis. The nemaline rod, then, would be constructed of 10 or more longitudinal subunits while normal Z bands have 2–4. A 3-D reconstruction of a very thin, one-subunit Z band from fish white muscle, however, showed an approximate twofold screw symmetry with two differing connecting links interior to the Z band (Luther, 1991), and a third set of "polar links" at the Z band edge. This thin Z band was expected to have a structure differing from that of the nemaline rod on the basis of a distinctly different appearance in electron micrographs of cross sections.

In the vertebrate skeletal and cardiac muscle, the 2–4-subunit Z band also exhibits an approximate fourfold symmetry in cross-sectional (parallel to the sarcomere axis) projection. In mammalian muscle, this fourfold symmetry is exhibited in two different structural states of the Z band (Reedy, 1964; Fardeau, 1969; Landon, 1970; Goldstein et al., 1990). The two structural states are called small square (ss)[1] and basket weave (bw) on the basis of the differing appearance of their cross-sectional projections. The two lattices exhibit characteristic Z band spacings as observed by electron microscopy, and each lattice form can be correlated with a different physiological state of the muscle (Goldstein et al., 1986, 1987, 1990). For instance, in rat soleus muscle, Z bands of unstimulated muscle exhibit the ss form, while muscles fixed in a state of tetanus exhibit the bw form. We have shown that this Z band lattice change is reversible in that muscles tetanized and then allowed to relax reveal the ss structure. Furthermore, the transition between Z band structural states requires activation of the muscle; it cannot be induced by forces exerted in a passive stretch (Goldstein et al., 1987).

Z band structural changes associated with muscle activation have been observed in other laboratories. In an x-ray diffraction study of intact fish muscle, Harford et al. (1994) observed an activation-induced change in the relative intensities of x-ray reflections from the I band/Z band region. This was not accompanied by a change in lattice spacing, however. Also, a study of strain-induced skeletal muscle failure (Tidball et al., 1993) showed that the breaking strength of the Z band varies with muscle activation.

We have investigated the 3-D structure of Z bands and I bands in unstimulated rat soleus muscle by tomographic reconstruction from an electron microscope tilt series of longitudinal sections rotated about the sarcomere axis. This tomographic technique does not use the crystallographic methods used in the earlier Z band reconstructions, thus allowing reconstruction of objects of potentially differing symmetry such as the Z and adjoining I and A bands.

The resulting Z band structures suggest that regions of protein density between the axial filaments must rearrange dynamically during contraction.

1. *Abbreviations used in this paper*: bw, basket weave; ss, small square; Z-RIB, Z band relaxed interconnecting body.

Materials and Methods

Preparation of Muscles

Sprague-Dawley rats (250–300 g) were anaesthetized by intraperitoneal injection of 50 mg kg^{-1} of Nembutal (Aldrich Chermical Co., Milwaukee, WI). The soleus muscle was dissected and tied to a wooden applicator stick, then removed from the leg and immersed in 2% glutaraldehyde in 100 mM Pipes buffer for 1 h at pH 7.2 at room temperature. Superficial fibers were cut into small cubes and returned to fresh fixative for an additional 2 h. Tissue samples were then rinsed in buffer for 2 h, postfixed in 1% osmium tetroxide in Pipes buffer, dehydrated rapidly in ethanol, and oriented and embedded in LX112 resin in flat silastic molds. The cured block was subjected to 2 min microwave radiation in a microwave oven to produce more stable specimens for EM.

Electron Microscopy

Semithin sections were stained with methylene blue-azure II and were examined with the light microscope to determine quality of fixation and proper orientation. Thin sections were cut on an ultramicrotome (MT-2B; Porter-Blum Research and Manufacturing Co., Tucson, AZ) by a diamond knife. Section thickness was estimated by noting the interference color of each section in a ribbon before positioning the ribbon onto the grid. Longitudinal sections intended for subsequent tilt series generation and 3-D reconstruction were selected for section thicknesses 100–120 nm (gold interference color). Cross sections had section thicknesses of 40–60 nm. For the longitudinal sections, the blocks were oriented with the long axis of the myofibers parallel to the knife edge. Z band width and sarcomere length of these sections were therefore minimally affected by compression. Colloidal gold beads (10-nm diam) were deposited on selected longitudinal sections by immersion.

Thin sections were examined in an electron microscope (201; Philips Electronic Instruments Co., Mahwah, NJ; or JEM200 CX; JEOL USA Inc., Peabody, MA) equipped with a goniometer. Single axis tilt series of longitudinal sections were recorded in the range +60 to −60 degrees in 1-degree increments at a magnification of 73,000. The tilt axis was approximately parallel to the myofibril axis. All tilt series specimens were allowed to stabilize in the electron beam for at least 15 min before collection of the tilt series data. Initial and final micrographs were taken at 0 degrees tilt to assess section stability during collection of the tilt series.

The microscopes were calibrated for all cross and longitudinal sections with a carbon grating (Ernest F. Fullam, Inc., Latham, NY). The sarcomere length was measured on longitudinal sections from the same block, imaged at ×3,000–×10,000, enlarged to a final magnification of at least 14,000, and expressed as a mean ± standard error. Cross section images used in another set of experiments (Goldstein et al., 1986) on the same animal were used for comparative measurement of the Z and A band spacings.

Optical Diffraction Analysis

Eight cross sectional electron micrographs of the same muscle used in 3-D reconstruction were selected for measurement of the Z and A d_{10} spacing by optical diffraction. Positives of these images were reduced from ×30,000 to ×18,000 and used as diffraction subjects, as described previously (Goldstein et al., 1986). Lattice dimensions of Z bands and adjacent A bands were measured directly from photographic recordings of the diffraction patterns. The system was calibrated by photographing a square grid of known spacing. No correction was made for section compression. Z spacings and A band d_{10} spacings were expressed as previously described (Elliott et al., 1967; Davey, 1976).

The contrast transfer function was examined by optical diffraction of electron micrograph negatives from the two tilt series to identify regions of comparable defocus (Radermacher, 1988; Hawkes, 1992). Areas showing occurrence of the first minimum of the phase contrast transfer function between 1.5 and 3 nm^{-1} were identified. Of these, areas containing a Z band were selected for digitization and subsequent 3-D reconstruction.

Image Processing

Image processing was done on computers (VAX 11/785; Digital Equipment Corporation, Marlboro, MA; and 4D-20 and 4D-25; Silicon Graphics, Mountain View, CA), using the SUPRIM (Bretaudiere et al., 1988; Schroeter and Bretaudiere, 1996) image processing software. Images were scanned with a digitizing camera (78/99; Eikonix Corp., Bedford, MA)

equipped with a regulated light source, and input to the computer as 1024 × 1024 × 12 bit arrays at a pixel size of 0.98 nm.

2-D image enhancement of the cross section images was performed as part of another experiment. The "lattice averaging" algorithm was also applied to cross sectional projections of the reconstructed Z bands (Schroeter et al., 1991), and an orientational search was performed to discover the tilt angles giving the best match to the enhanced cross section images.

3-D reconstruction of the Z band and of the nearby I and A bands was performed using weighted back projection techniques (Hoppe and Hegerl, 1980; Radermacher et al., 1987). First, the digitized tilt series micrographs were aligned translationally and rotationally using the center of mass of 10–20 gold beads (~10 nm diam) as fiducial marks (Lawrence, 1992; Schroeter and Bretaudiere, 1996). 128 × 128 pixel images of corresponding regions were automatically extracted from the set of aligned images using software written in-house. Some of the automatically extracted images fell outside the transfer function criterion, or were not inside the frame on each micrograph in the series. These images were discarded from the tilt series for the region. The remaining tilt series images for each region were then padded to 256 × 256 to avoid aliasing effects, Fourier transformed, and weighted in Fourier space by the appropriate "sinc" function filter (Radermacher et al., 1987). The images were then inverse transformed, unpadded to the original size, and combined into initial 3-D reconstructions by back projection. The translational and in-plane rotational parameters for each projection in the tilt series were refined further using a method similar to that of Penczek et al. (1994). After refinement of the orientational parameters, the tilt series images were weighted and recombined into final 3-D reconstructions. Model Z and I band lattices in the same orientation as that in our reconstructions were projected to form test tilt series images. These images were subjected to a small rotational and translational misalignment and reconstructed to demonstrate that the described procedure successfully reproduced the lattices.

The resolution of the reconstructions was assessed by back calculation from the measured thickness of the reconstructed section (Crowther et al., 1970) and by calculation of the phase residual (resolution cutoff = 45 degrees) in a spherical shell that included the missing wedge (Frank et al., 1981). The final 3-D reconstructions were low-pass filtered to the worst case resolution of 5 nm. No correction was made for section compression or shrinkage.

Image Analysis

The reconstructed volumes were displayed as projections in false color, as shaded solids, and as contoured slices using the SUPRIM and SYNU (Hessler et al., 1992; Schroeter and Bretaudiere, 1996) image display facilities. The contour level selected for the projected images was that which best matched the input electron micrographs. For the shaded solid images, the contour level was adjusted to the point at which the axial filaments became distinct from the surrounding amorphous matrix. Projections of cross sections through the reconstructions of the Z and I band reconstructions were examined, and the Z band spacings for the reconstructions were measured directly on printouts and by examination of power spectra. Projections of longitudinal sections through the reconstructions were also examined, and the spacing between projected longitudinal filaments was measured directly, and where possible, by examination of power spectra.

Sections taken from the reconstructions were rendered as shaded solids in stereo, so that individual axial filaments could be traced through the Z band. The distances between successive cross connections to each traced axial filament were measured directly on printouts of the rendered objects. These data were collected for successive coplanar cross connections as well as for orthogonal cross-connecting filaments. Additionally, axial filament diameters were measured as the width of the filament profile in the (1,0) or (0,1) orientation at the center of the Z band and in the I band 40 nm from the Z–I boundary.

Results

Resolutions

We have reconstructed six different Z band regions from our one degree increment tilt series of a region containing two Z bands. Additionally, six I band regions adjoining the Z band were reconstructed from this series. The resolution of these reconstructions was estimated from Fourier space considerations (Crowther et al., 1970; Frank and Radermacher, 1986; Radermacher, 1992) as ranging from three to five nm. The resolution was also measured by calculating the phase residual as in a spherical shell in Fourier space (Frank et al., 1981). These resolutions ranged from 3.4 to 13 nm.

Of the 12 reconstructions of parts of the muscle, not all were found to be suitable for structural analysis. Only four of the six Z band reconstructions showed evidence of a regularly repeating lattice in cross section, while the other two exhibited greater disorder. Of those with a repeating lattice, two Z band reconstructions exhibited resolutions >8 nm, leaving two Z band reconstructions with resolutions of 4.3 and 3.4 nm that were deemed suitable for analysis. Similar attrition effects reduced the number of I band reconstructions used in the analysis to four, with resolutions of 3.4, 4.8, 3.7, and 4.4 nm. Therefore we have low-pass filtered the analyzed reconstructions to 5 nm.

Two-Dimensional Projections

Fig. 1 shows an electron micrograph of a longitudinal section of the unstimulated rat soleus muscle used for subsequent 3-D reconstruction. The Z band is ~100 nm wide. This corresponds to approximately three of the repeating units seen in longitudinal projections (Goldstein et al., 1980, 1990), and is characteristic of this fiber type. Sarcomere lengths were measured from a number of longitudinal sections of this muscle and averaged 2.5 ± 0.2 μm. In this and the subsequent Figs. 2–4, protein appears dark against a light background.

Fig. 2 shows a cross-sectional image from the same muscle. The projected Z band lattice in this cross section exhibits the small square pattern expected in unstimulated rat soleus muscle (Goldstein et al., 1986, 1990). In the figure, a small portion of this lattice has been outlined to guide the eye. Optical diffraction measurement of the Z band lattice dimensions gave a Z spacing of 20.4 ± 1.0 nm, n = 24, (mean ± SD), consistent with previous measurements from electron microscopy (Goldstein et al., 1986).

A projection of a longitudinal section through one of the reconstructed Z bands is shown in Fig. 3 *a*. This section includes regions with the "chevron" or (1,0) orientation of the longitudinal Z band (Goldstein et al., 1977; Morris et al., 1990). A power spectrum of this section reveals a longitudinal spacing of 37.7 nm consistent with measurements from EM longitudinal sections (Goldstein et al., 1980). Fig. 3 *b* shows the same region from one of the micrographs used to calculate the reconstruction. Fig. 3 *c* shows a cross-sectional projection taken through the central 40 nm of the reconstruction shown in Fig. 3 *a*. A power spectrum of this section gives a Z band lattice spacing of 20.5 nm, consistent with our previous measurements from electron micrograph cross sections exhibiting the small square pattern (Goldstein et al., 1986). For comparison, a similarly sized region selected from the Fig. 2 micrograph of a Z band cross section is shown in Fig. 3 *d*. In the two cross sections, a portion of the lattice has been outlined to guide the eye. The outlined lattices are easily visualized by viewing the figure at a glancing angle. Note that the reconstructed lattice (Fig. 3 *c*) shows a diamond shaped unit cell, while the other lattice (Fig. 3 *d*) is more square. We have

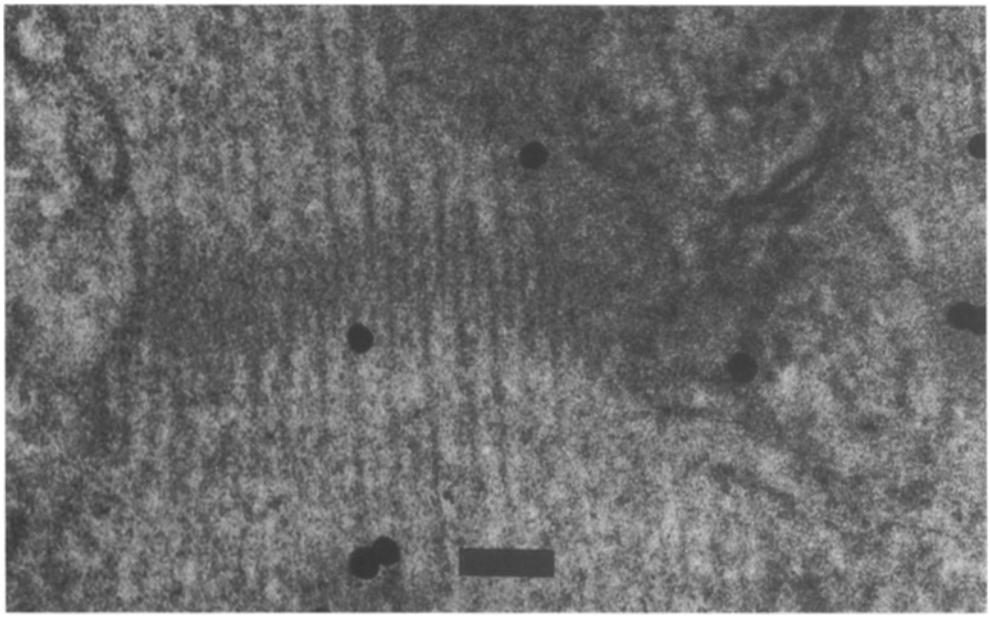

Figure 1. Electron micrograph of a longitudinal section of unstimulated rat soleus muscle. The black circular objects are gold particles that were deposited on the section for use as fiducial marks. In this micrograph, muscle filaments appear dark against a light background. Bar, 50 nm.

observed previously such diamond-shaped lattices in cross-sectional electron micrographs of Z bands from unstimulated muscle (Goldstein et al., 1982). Fig. 3 *e* shows a 2-D–enhanced image of all of the reconstructed cross section displayed in Fig. 3 *c* produced by lattice averaging. A similar enhancement of the Z band cross section of Fig. 3 *d* is shown in Fig. 3 *f*. The characteristic cross-sectional projection of the small square lattice is seen in both figures. In these enhanced projections, four axial filaments (X) from one sarcomere surround a nearest neighbor axial filament from the opposite sarcomere (+). Four cross-connecting Z-filaments appear to connect each axial filament to its four nearest neighbors. The cross-connecting filaments join or overlap in projection at a region of greater density (o) approximately halfway between the cross-cut axial filaments.

Cross Sections of the Reconstruction

Cross-sectional projections taken through the I band and the Z band from another set of reconstructions are shown

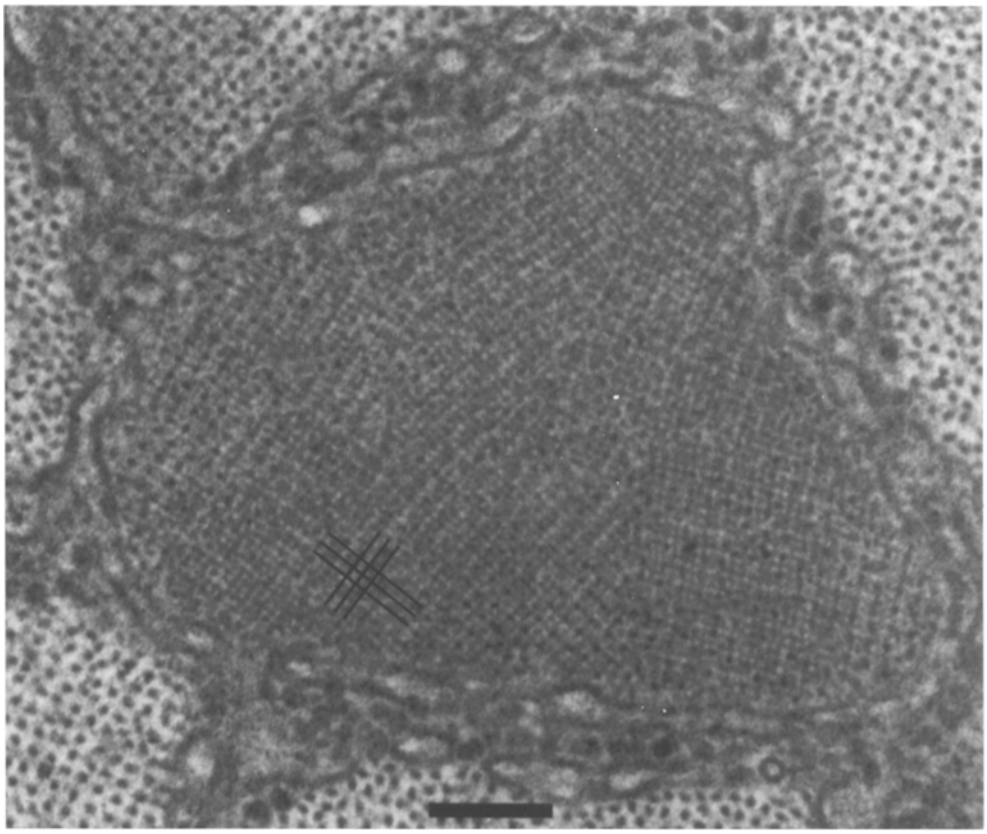

Figure 2. A digitized electron micrograph of a cross section from the same muscle and block as Fig. 1. The Z band exhibits the small square lattice pattern expected in unstimulated rat soleus muscle. A small portion of the small square pattern has been outlined to guide the eye. Once again, protein-dense regions appear dark against a light background. Bar, 100 nm.

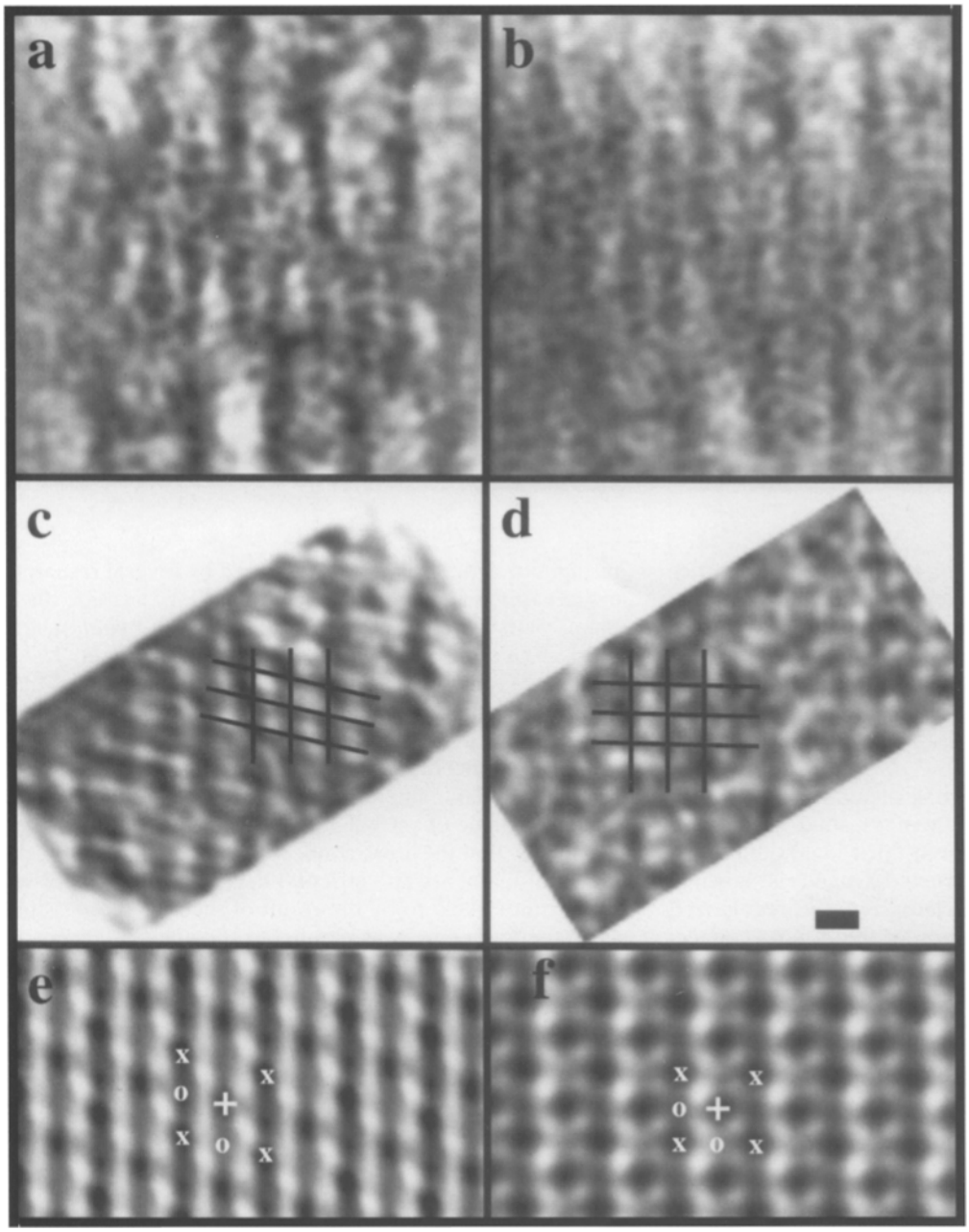

Figure 3. 2-D projections of the Z band and nearby I band. (*a*) A longitudinal projection of a 30-nm thick section through a 3-D reconstruction of the Z band and nearby I band. (*b*) For comparison, an electron micrograph of the same region. The interconnecting filaments in the Z band appear more distinct in the thinner section from the reconstruction. (*c*) A cross-sectional projection taken through the central 40-nm region of the reconstruction shown in longitudinal projection in *a*. The expected small square appearance of the Z band lattice is visible in this projection, and a small region of the pattern has been outlined to guide the eye. This section is tilted so that the longitudinal projection in *a* would be seen by a viewer looking down on the reconstruction from the top of this figure. (*d*) For comparison, an electron micrograph of a similarly sized and oriented region of the small square pattern from Fig. 2. (*e*) A 2-D enhanced image of the region of the reconstructed Z band lattice shown in *c*, produced by "lattice averaging". (*f*) For comparison, a similar enhancement of the Z band region shown in *d*. In both enhancements, cross-cut axial filaments from one sarcomere (*x*) surround axial filaments from the opposite sarcomere (+). Cross-connecting Z-filaments form a fourfold array in these projections, seeming to join or overlap at a region (*o*) between the axial filaments. In this, as in all other projection images, protein appears dark against a white background. Bar, 10 nm.

in Fig. 4. As in Fig. 3 *c*, these images are projections of the reconstruction parallel to the sarcomere axis, and thus correspond to electron micrograph of cross sections of the muscle. The figure displays a group of cross sections taken through the reconstructed Z band and nearby I band. The position of a single filament (+) has been followed through the sections. Far from the Z band, the I band appears disordered with little evidence of a fourfold arrangement of the cross-cut thin filaments in a 20-nm-thick section (Fig. 4 *a*). Nearer the Z band (Fig. 4 *b*), a 20-nm-thick I band cross section exhibits the large-square appearance described in previous studies (Landon, 1970; Goldstein et al., 1982; Yamaguchi et al., 1985). The gray lines are drawn to outline the somewhat distorted large square. Inside the Z band, a 20-nm-thick cross section exhibits the small square pattern expected on the basis of previous studies of relaxed rat soleus muscle (Fig. 4 *c*). Here, the grey lines are drawn to emphasize a small part of the ss lattice. Surprisingly, patches of the ss pattern are visible in a thin 2-nm section (Fig. 4 *d*) cut from the central region of the

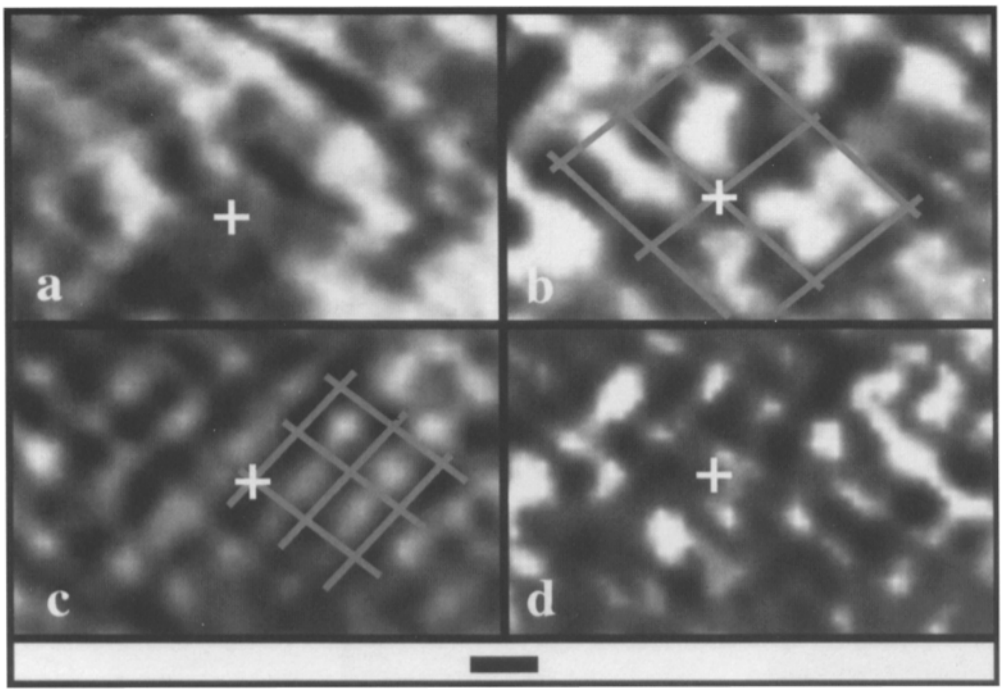

Figure 4. Cross-sectional projections of another reconstruction in parts of the I and Z bands. A origin filament (+) is indicated in all four projections. Unless otherwise stated, the cross sections were 20 nm thick. (*a*) As far as 80 nm from the Z band, a cross-sectional projection shows little evidence of four-fold symmetry. (*b*) Nearer to the Z band, the I band shows patches of the large square lattice pattern (*gray lines*). (*c*) Inside the Z band, the small square pattern is visible. A small region of this pattern has been outlined in gray. (*d*) In the Z band the small square pattern can be observed in sections as thin as 2 nm. The outlined lattices may be visualized more clearly by viewing this figure at a glancing angle. Bar, 10 nm.

section shown in Fig. 4 *c*. Thus, the small square lattice pattern can be generated by projection of a cross section much thinner than the ~38-nm longitudinal repeat seen in optical diffraction studies of Z band longitudinal sections (Goldstein et al., 1980).

Shaded Surface Display

In addition to displaying the reconstructed volumes in projection, we may also render them as solid objects. A shaded solid rendering of a 14-nm-thick longitudinal section through one of the reconstructed Z bands is shown in Fig. 5 *a*. For comparison, a skeletonized and regularized model depicting our interpretation of the Z band connectivity is shown in Fig. 5 *b*. In these figures, different Z and I band structural elements have been rendered in different colors. In Fig. 5 *a*, vertical axial filaments enter the Z band from the top (*yellow*) and bottom (*orange*) of the figure. As the axial filaments enter the Z band, cross-connecting Z-filaments appear (*blue*), and the axial filaments sometimes seem to bend or terminate at the connection points. Some of the axial filaments appear to decrease in diameter upon entering the Z band (see especially the central orange filament, Fig. 5 *a*). This is consistent with the measured diameters of 10 ± 2 nm (n = 19) in the Z band and 14 ± 4 nm (n = 20) in the nearby I band. Each axial filament continues through the Z band, terminating before or at the edge of the I band on the opposite side. It is apparent that the axial filaments from opposite sarcomeres interdigitate in the Z band, as described by several researchers (Knappeis and Carlsen, 1962; Kelly, 1967). Inside the Z band, pairs of cross-connecting Z-filaments (*blue*) bind most often on opposite sides of each axial filament. There are two to four such binding regions along each axial filament inside this particular reconstruction. This figure, as well as Fig. 3, *a* and *b*, shows that the connection points for the cross-connecting Z-filaments are displaced axially on successive axial filaments. These points define a line which makes an angle of ~10 degrees with the horizontal in this Z band, so that the cross-connecting filaments do not meet the axial filaments at a strict 90 degree angle. This offset angle is not likely to be the result of section compression, since the knife edge was parallel to the myofibril axis and thus perpendicular to the plane of the cross-connecting filaments. It must be noted, however, that the precise numerical value for the offset may be affected by compression artifacts. When nonzero offset angles are observed, the value may range from ~5 to ~15 degrees. Such values for the offset angle have been observed in longitudinal sections of canine cardiac muscle, and in Z rods (Goldstein et al., 1977).

As one travels along a given axial filament inside the Z band, the cross-connecting Z-filaments are seen to lie in two approximately orthogonal planes. These planes are the planes of projection for the chevron orientations of the Z band, that is, the (1,0) and (0,1) orientations. Often, the orthogonal cross-connecting filaments join the axial filament near the same point. Thus, in these regions, four

Figure 5. Shaded solid renderings of sections of 3-D reconstructions of the Z band compared with regularized and skeletonized models. (*a*) A 14-nm thick longitudinal section of one of the reconstructed Z bands shows the interdigitating axial filaments and the cross-connecting Z-filament array. Axial filaments enter the Z band from the top (*yellow*) and bottom (*orange*) of the figure. The filaments are joined together by cross-connecting Z-filaments (*blue*) which also connect to the filamentous relaxed interconnecting body or Z-RIB (*red*). In the I band near the top and bottom of the figure, some connections run directly between the axial filaments (*magenta*). Amor-

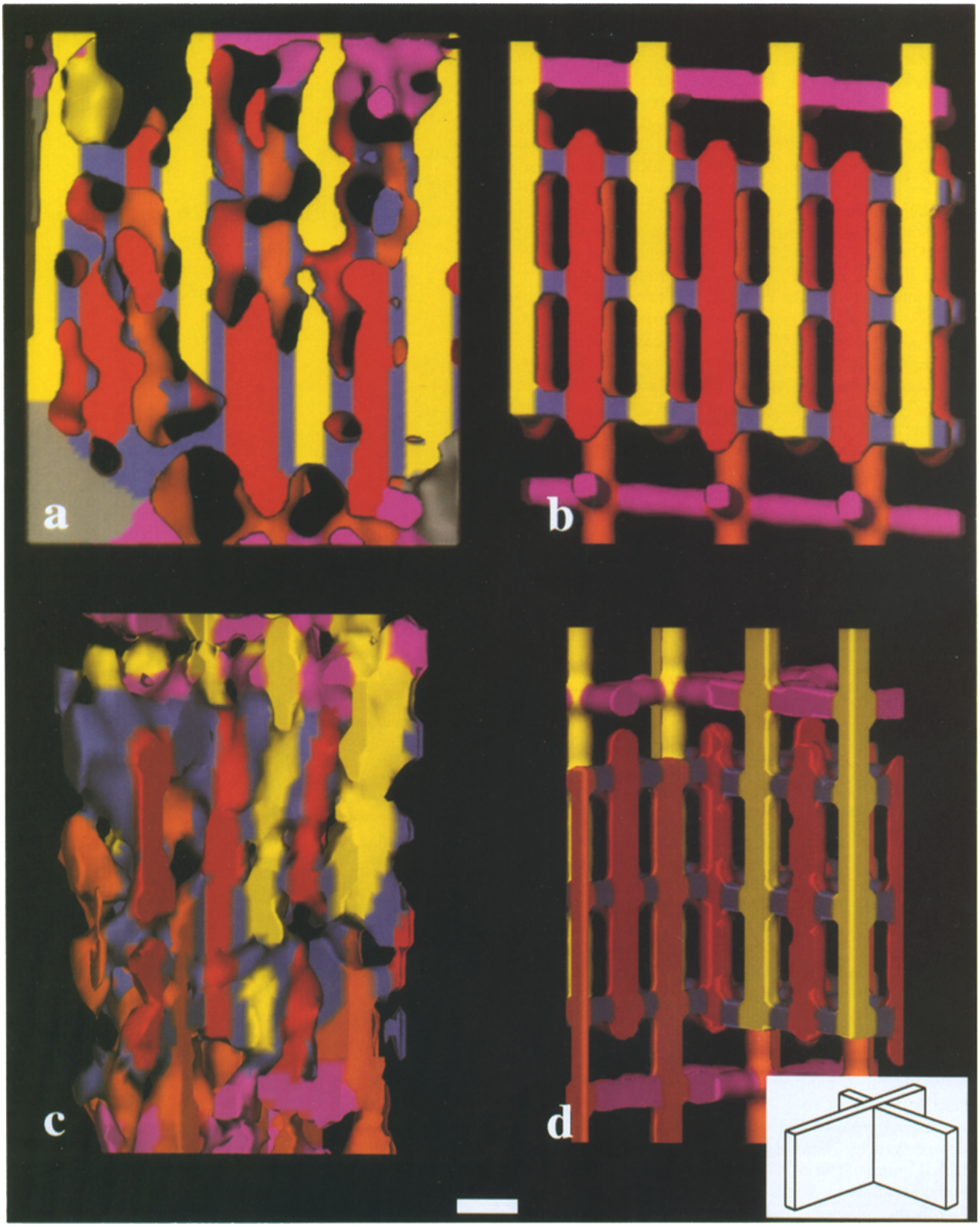

phous material (*gray*) obscures the filaments near the bottom corners of this section. (*b*) A regularized skeletal model showing our interpretation of the connectivity seen in *a*. In this model, the ~10 degree axial offset is shown by the blue cross-connections, which run at an angle to the horizontal. This angle has been decreased somewhat for clarity. (*c*) The region of intersection of two 7-nm thick longitudinal sections through one of our reconstructions, showing interruptions in the Z-RIB (*red*). (*d*) A model of the region shown in *c*. The inset diagrams the arrangement of the intersecting slabs in *c* and *d*. Bar, 10 nm.

cross-connecting filaments join the axial filament in the same or nearly the same cross-sectional plane. Less often, only two opposing cross-connecting filaments are seen to meet the axial filament. The cross-connecting filaments connect to or form a vertical Z band relaxed interconnecting body (Z-RIB) which lies between the axial filaments and is shown in red. Several instances of this body are visible in Fig. 5, *a* and *c*. Fig. 5 *c* shows a shaded solid rendering of the region of intersection between two quite thin (7 nm thick) longitudinal sections that are approximately perpendicular to one another. For comparison, a skeletonized and regularized model of the intersecting slabs is shown in Fig. 5 *d*, while the inset diagrams the positions of the two intersecting slabs of Fig. 5, *c* and *d*. The central Z-RIB of Fig. 5 *c* traverses the full width of the Z band, while those to either side exhibit vertical interruptions. These gaps in the relaxed interconnecting body are also seen in Fig. 5 *a*, near the left side of the figure. Also notice that the Z-RIB sometimes appears to extend beyond the ends of the axial filaments.

The increased density often observed in the Z band occurs in longitudinal projections of our reconstructions despite a modest decrease in the diameter of the axial filaments as they enter the Z. Thus, the increase in projected density is seen to be due to the interdigitation of axial filaments from opposite sarcomeres as well as the presence of the dense net of cross-connecting Z-filaments associated with the relaxed interconnecting body.

Some cross-connecting filaments joining the I band thin filaments are visible near the top and bottom of Fig. 5 (*magenta*). These filaments have been previously observed in electron micrographs of the I and Z bands (Trombitas et al., 1988; Tskhovrebova, 1991), and are ubiquitous in our I band reconstructions (see below).

Orientation and Distances between Cross Connections in the Z and I Bands

The distance along the axial filament between cross-connecting Z-filaments lying in the same plane was measured for each axial filament. A histogram of the measurements (Fig. 6 *a*) reveals a pronounced peak for distances <5 nm. This peak corresponds to regions where pairs of cross-connecting Z-filaments join to opposite sides of the axial filament. A second peak in the histogram occurs near 20 nm. If the distances <5 nm are neglected, the average distance between these coplanar connecting points becomes 26 ± 10 nm (n = 90).

The histogram of distances measured along the axial filament between Z band cross connections oriented ~90 degrees with respect to one another is shown in Fig. 6 *b*. Like the histogram of Fig. 6 *a*, the distances show a secondary peak at 15–20 nm. However, the histogram also reveals that many of the cross connections occur 5 nm or less from the attachment points of orthogonal filaments. Coupled with the near zero peak seen in the coplanar histogram, this implies that as many as four cross-connecting Z-filaments can join the axial filament in a distance along the filament ≤5 nm. This is consistent with the observation of regions of the small square lattice pattern in the 2-nm cross section of Fig. 4 *d*. The average distance between the orthogonal Z band cross connections was 14 ± 13 nm (n = 50), or 18 ± 12 nm (n = 37) if the peak near zero is neglected.

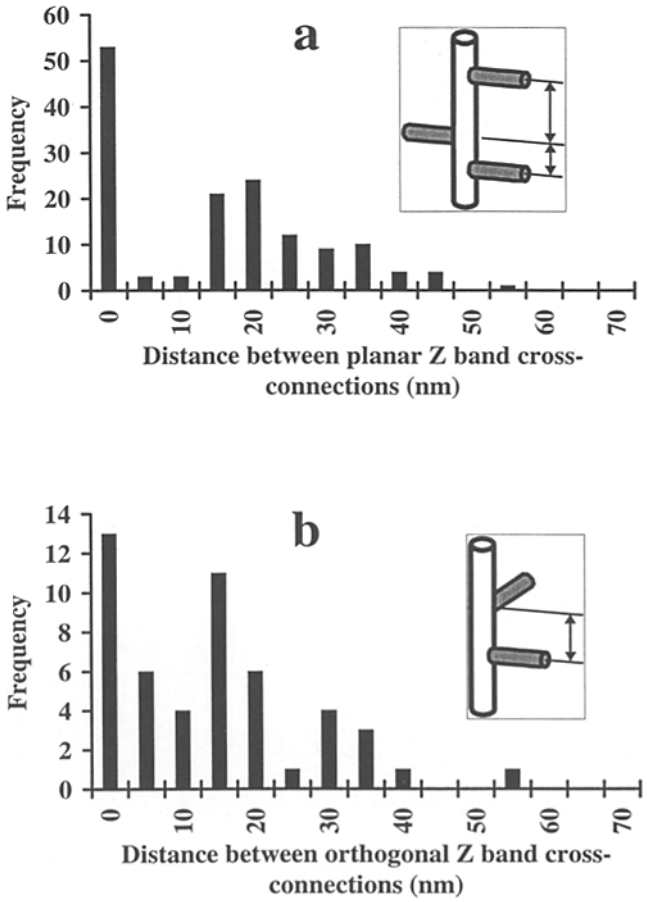

Figure 6. Histograms of distances between cross-connecting Z-filament attachment points along an axial filament in the Z band. (*a*) Distances in the Z band between attachment points for cross-connecting Z-filaments lying in the same longitudinal plane, that is, the plane formed by the axial filament and one of its nearest neighbors. The inset indicates how these distances are identified. (*b*) Distances in the Z band between binding points for cross-connecting Z-filaments that lie in approximately orthogonal longitudinal planes. The inset shows how these distances are identified.

In the I band reconstructions located within ~80 nm of the I–Z junction cross-connecting filaments are observed to join the thin filaments. The arrangement of the connecting points appears similar to that in the Z band, and has been analyzed in the same way. Along an axial filament, cross-connecting filaments in the same plane average a distance of 28 ± 9 nm (n = 123) apart, if the near zero distances due to opposing pairs are neglected. Orthogonal filaments average 14 ± 10 nm (n = 47) apart for the full data set, or 16 ± 9 nm (n = 37) if the distances <5 nm are neglected. The histograms of the data shown in Fig. 7 reveal distributions quite similar to those seen in the Z band. In particular, both histograms show pronounced peaks near zero and secondary peaks at 15–20 nm. This is evidence for a similar distribution of potential connecting sites in the Z and I bands.

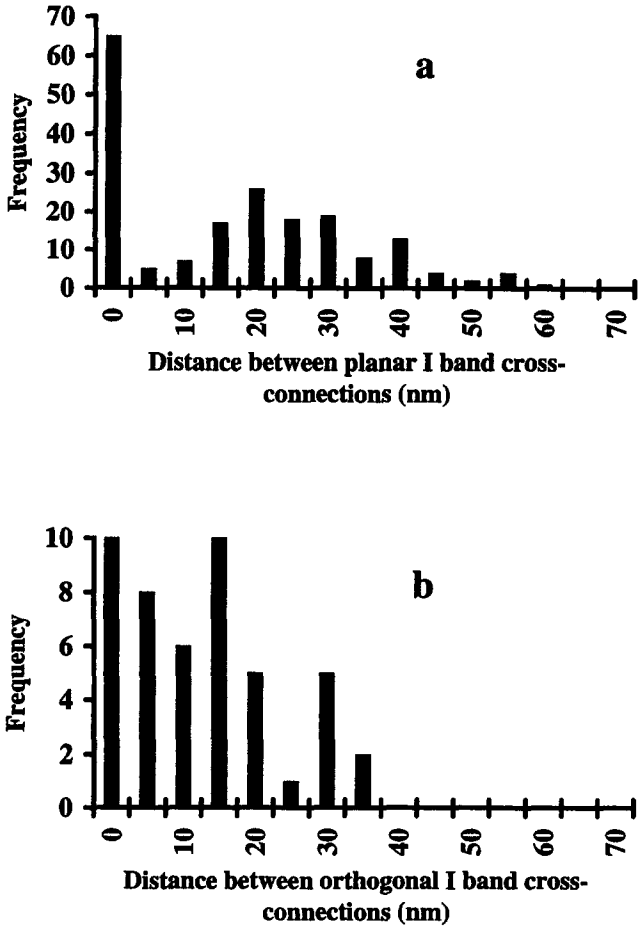

Figure 7. Histograms of distances between attachment points along an axial filament, for cross connections in the I band. These distances were measured within 80 nm of the I–Z junction. (*a*) Distances in the I band between binding points for cross connections in the same longitudinal plane. (*b*) Distances in the I band between binding points for cross connections in approximately orthogonal longitudinal planes.

Discussion

In our unstimulated rat soleus muscle Z band reconstructions, the Z band consists of two or three longitudinally stacked repeating units. These repeating units approximate parallelopipeds with longitudinal dimension averaging 26 ± 10 nm and approximately equal cross-sectional dimensions of 20 ± 3 nm. The histograms of longitudinal spacings between planar and orthogonal cross-connecting Z-filaments (Fig. 6) suggest the structure of the repeating unit. The peaks near zero spacing indicate that as many as four cross-connecting filaments may join the axial filament within a 5-nm distance. The shaded solid renderings (Fig. 5, *a* and *c*) show that, sometimes, only one filament may bind in a particular region. The 2-nm cross-sectional projection of Fig. 4 *d* shows that the four-connection binding dominates the current reconstructions. A schematic of the Z band and nearby I band demonstrates this connectivity between interdigitating pairs of axial filaments (Fig. 8 *a*). This schematic is oriented similarly to the renderings of Fig. 5, *c* and *d*. In the schematic, four cross-connecting Z-filaments (*dark gray in figure*) bind to the axial filaments (*white*) in an arrangement of orthogonal pairs. The fourfold connecting filament binding sites are separated by 15–20 nm along the axial filament. This spacing is consistent with the 15–20-nm peaks seen in the histograms of Fig. 6. This connectivity generates the small square lattice in cross section with the Z-RIB (*dark and white vertical rods*) joined to or formed by the connecting filaments providing the region of higher density between the cross-cut axial filaments. If the Z-RIB is formed by the cross-connecting Z-filaments, they would be forced to take the rather tortuous path indicated in the schematic (*arrows*). This path is similar to that suggested by Morris (Morris et al., 1990) for the nemaline rod. The relaxed interconnecting body often traverses the complete Z band, with the gray and white vertical rods in the figure forming a continuous path. However, we also observe Z band regions where one or more of the vertical rods in the figure are absent (see also Fig. 5, *a* and *d*). The Z-RIB is also shown to extend vertically beyond the ends of the axial filaments, as seen in Fig. 5.

An alternative connectivity is implied by the average values for the longitudinal distances between cross connections. The 26 ± 10 nm average distance measured between coplanar connecting filament pairs along the axial filament is about a standard deviation less than the ~38-nm longitudinal repeat seen in the power spectrum of longitudinal projections of our Z band reconstructions. This "ordered" repeat distance is similar to the 36-nm pseudo repeat of F-actin and to optical diffraction results from electron micrographs of longitudinal sections (Huxley and Brown, 1967; Goldstein et al., 1977; Holmes et al., 1990). The 14 ± 13– or 18 ± 12–nm average distances measured between orthogonal cross connections are well within a standard deviation of one-half of the ordered repeat. Thus, these average distances are consistent with a structure exhibiting an ~38-nm distance between coplanar filament pairs, and ~19 nm between orthogonal cross connections. If such a relationship is postulated, it leads to a connectivity like that schematized in Fig. 8 *b*. In that figure, opposing pairs of cross-connecting Z-filaments bind to the axial filament. Successive pairs bind in planes rotated 90 degrees about the axial filament. This arrangement exhibits a fourfold screw symmetry similar to that seen in the nemaline rod (see below).

In the actual reconstructions, each repeating unit is seen to vary in a greater or lesser degree from its neighbors. Disorder is apparent in that the axial filaments do not always traverse the complete width of the Z band and may also bend at cross-connecting points. Further, the cross-connecting Z-filaments do not meet successive axial filaments in the same cross-sectional plane. Thus, nearest neighbor axial filaments have cross-connecting filament-binding sites that are longitudinally offset from one another. The binding sites follow a line ~10 degrees from the horizontal in the chevron orientations displayed in Fig. 3, *a* and *b* and Fig. 5 *a*.

In the I band near the I–Z junction, filaments are observed to connect the axially directed thin filaments into a disordered large square array. These are shown as white horizontal rods in the schematics of Fig. 8. As in the Z band, the I band–connecting regions may have up to four cross-connecting filaments binding within <5 nm, as im-

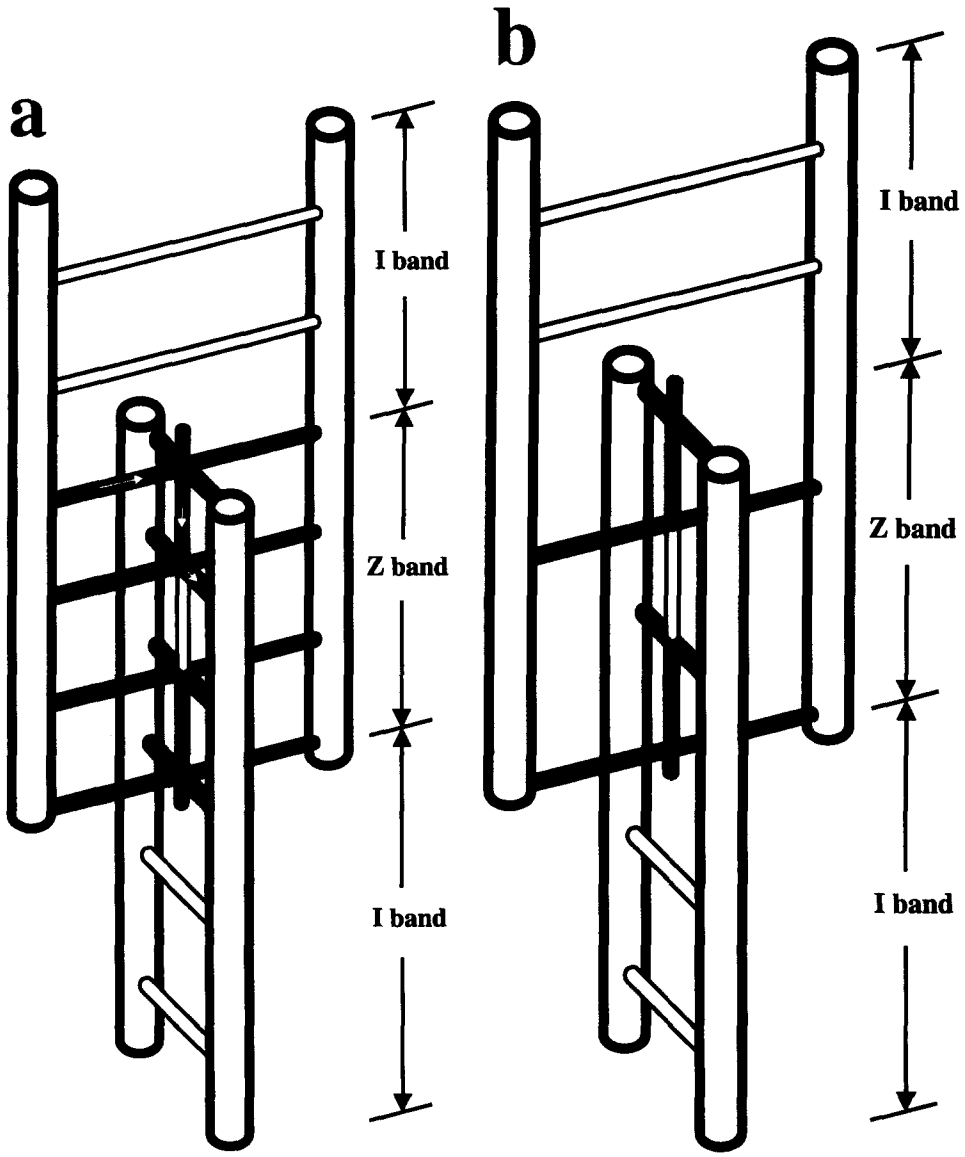

Figure 8. Schematic of the Z band and nearby I band. Opposing pairs of axial filaments are shown as large diameter vertical white rods. In the Z band, they are linked by cross-connecting Z-filaments (*dark gray horizontal rods*) which form or connect to the Z band relaxed interconnecting body or Z-RIB, shown as dark and white vertical rods. I band cross-connecting filaments are shown as white horizontal rods. (*a*) The structure observed most often in our Z band reconstructions. White arrows indicate a possible path cross-connecting Z-filaments might take in producing the observed structure. (*b*) The structure constructed using the average distances between cross-connecting Z-filaments. The orientation of this schematic is similar to that of Fig. 5, *c* and *d*.

plied by the histograms of Fig. 7. Furthermore, the distances between coplanar and orthogonal connections show a similar statistical behavior to that seen in the Z band (compare Fig. 6 *a* with Fig. 7 *a* and Fig. 6 *b* with Fig. 7 *b*). Thus, the difference between the array of cross connections in the Z band and in the nearby I band is primarily the presence of the relaxed interconnecting body in the Z. This implies that the Z-RIB in the Z band may exist as a separate entity, rather than simply as part of a cross-connecting Z-filament.

The lengths and diameters of the Z band filaments observed in the reconstruction are consistent with known Z band components. The axial filaments have an F-actin core (Yamaguchi et al., 1983*b*; Zimmer and Goldstein, 1987*a*), and in the Z band appear to be covered by α-actinin (Tokuyasu et al., 1981; Zimmer and Goldstein, 1987*b*). The ~10-nm diameter of the axial filaments in our reconstruction is consistent with this axial filament structure. α-Actinin, a filamentous protein dimer with a diameter of ~3 nm and a length of 40 nm is a known component of the cross-connecting Z-filaments (Podlubnaya et al., 1975; Reedy et al., 1975; Zimmer and Goldstein, 1987*b*). Furthermore, in vitro experiments have demonstrated that α-actinin can connect neighboring F-actin strands with an axial spacing like that seen in Z bands (Tskhovrebova, 1991). If the cross-connecting Z-filaments follow the bending path shown in Fig. 8 *a*, the distance traversed between axial filaments would be 40–50 nm. The distance traversed between axial filaments in the case of a direct cross connection from axial filament to relaxed interconnecting body to axial filament is only ~10 nm. Thus, the α-actinin dimer would be forced to wrap around or lie along the axial filament for a distance of 15 nm at each end for the direct connection to be geometrically feasible. Such a geometry would be consistent with the observation that the axial filaments are covered by α-actinin in the Z band.

The average Z band structure schematized in Fig. 8 *b* contains a relaxed interconnecting body and four connections between it and axial filaments from opposite sarcomeres in one longitudinal subunit. A Z band containing a single longitudinal subunit of this type would therefore yield a zig-zag longitudinal projection similar to that observed in

the thinnest Z bands (Franzini-Armstrong, 1973; Luther, 1991). Such a zig-zag longitudinal projection would not be as easily generated by the structure shown in Fig. 8 *a*. Nevertheless, this structure seems to represent the most common connectivity seen in our reconstruction, and might be called the "mode" structure, as opposed to the "average" structure of Fig. 8 *b*. For either of these structures, addition of subunits along the myofibril axis could construct a Z band of any width that is a multiple of the height of the subunit, accounting for the widened (up to 1,200 nm) Z bands seen in nemaline myopathy (i.e., the nemaline rod) and in aging dog heart (Goldstein et al., 1977, 1980).

Electron micrographs of the nemaline rod show a similar lattice structure to that seen in 2-D projections of the unstimulated rat soleus Z band. In particular, the small square lattice pattern is observed in cross sections of both. The nemaline rod shows a pronounced crystalline order over much longer distances than is observed in the rat soleus Z band. Since the nemaline rod disrupts the structure of the normal sarcomere, this increased ordering may be due to the absence of the normal force transmitting connections between the Z, I, and A bands. However, a 3-D reconstruction of the nemaline rod by Morris, Nneji, and Squire (Morris et al., 1990) is quite similar to the present reconstruction. The nemaline rod reconstruction was performed by direct Fourier techniques on the highly ordered nemaline rod, so that the unit cell produced is an average over a large portion of the nemaline rod. The average unit cell showed a fourfold screw symmetry of the cross-connecting Z-filaments similar to the behavior (Fig. 8 *b*) postulated on the basis of the average interconnection distances measured in the current reconstruction. In agreement with the rat soleus Z band, the axial filaments from opposite sarcomeres were found to interdigitate, with four filaments from one sarcomere surrounding one from the opposite sarcomere. Furthermore, the cross-connecting Z-filaments were seen to form a connecting structure that would contain the Z-RIB seen in the present reconstruction.

However, the nemaline rod reconstruction showed no evidence for attachment of more than two cross-connecting Z-filaments within a short 5-nm region along the axial filament. Also, the Z-RIB is often observed to be continuous through the Z band in the present reconstruction (Fig. 5, *a* and *c*), while the nemaline rod reconstruction reveals a regular interruption in the corresponding structure between every other layer of cross connections. Additionally, the nemaline rod reconstruction shows axial filaments with a diameter of 15–17 nm, as compared with the 8–12 nm seen in the Z band reconstruction. In the rat soleus Z band reconstructions, the axial filaments are seen to kink or sometimes terminate near Z band cross-connecting points. Most of the axial filaments, however, seem to traverse the entire distance to the opposite I–Z junction, in agreement with the nemaline rod reconstruction. Finally, the ~10 degree axial offset between connecting points on neighboring axial filaments was not observed in the nemaline rod reconstruction. It should be noted, however, that this offset is not always observed in longitudinal projections of the nemaline rod (Goldstein et al., 1980).

Luther (1991) has completed a 3-D reconstruction of a very narrow Z band from unstimulated fish white muscle, using techniques similar to those for the nemaline rod. This Z band is highly ordered in cross section, and represents perhaps the simplest Z structure since it reveals a single zig-zag structure in longitudinal section, with little interdigitation of the axial filaments. In cross section, this Z band exhibits a lattice pattern closely related to the bw pattern seen in tetanized rat soleus muscle. In the fish muscle reconstruction the two sets of cross-connecting filaments, termed the proximal and distal links, are rotated with respect to one another by ~80 degrees about the axial filament. They join or bind to the axial filament at attachment points within 5–15 nm along the axial filament. The links directly connect interdigitating axial filaments from opposite sarcomeres. Each axial filament is also connected to two other axial filaments from the same sarcomere by a "polar link," which may be similar to the I band cross connections observed in the rat soleus Z band. No interconnecting body is visible in the central region of the Z band. x-ray diffraction studies of a closely related fish muscle show evidence for a structural change in the region including the Z band upon activation of the muscle (Harford et al., 1994). Unlike rat soleus muscle, this change is not accompanied by an apparent expansion in the Z band lattice. However, this observation could result if the muscle exhibits large patches of the bw structure in the resting state. The existence of such patches is suggested by the large 29-nm Z band spacing observed, as well as by the bw-like Z band structures observed in electron micrographs of the similar plaice fin muscle (Harford et al., 1994) and *Rutilus rutilus* white muscle (Luther, 1991).

A major difference between both the nemaline rod and fish muscle Z band reconstructions and the present reconstructions from rat soleus muscle is the much greater disorder seen in the rat soleus structure. This greater disorder results in a large part from the absence of averaging in our reconstruction by the weighted back-projection technique. This technique does not impose a crystalline symmetry on the reconstruction, and no average unit cell is generated. Hence, the region reconstructed is a particular portion of the somewhat disordered Z band lattice (see Figs. 1 and 2). It is also possible that some of the disorder in the reconstruction is a result of the unstimulated rat soleus Z band not uniformly exhibiting the ss lattice form. This conjecture is consistent with the observation of small bw patches in cross sections of unstimulated rat soleus muscle (Goldstein et al., 1982).

Irving and Millman (1992) have stated that structural information derived from electron microscopy may be inaccurate due to unpredictable amounts of differential shrinkage of the A and Z bands during preparation for EM. This suggestion is offered to explain the 17–25% discrepancy between EM measurements of A band and Z band lattice spacings and Z/A ratios in intact rat soleus muscle and comparative results from x-ray diffraction studies of skinned and intact frog sartorius muscle. Two previous studies in frog (Yu et al., 1977) and in fish (Harford et al., 1994) show agreement between lattice spacings and ratios derived from microscopy and diffraction. We speculate that the different observations in frog and rat may reflect real differences in lattice spacing between the two muscles.

Some workers have observed "elastic" filaments (titin), connecting the skeletal muscle Z band to other parts of the sarcomere (Wang and Ramirez-Mitchell, 1983; Fürst et al.,

1988). There is little evidence of these filaments in our reconstruction. It may be that they are simply too small in diameter to be visible in our ~5-nm resolution structure. If these filaments do connect to the Z band, a likely candidate for the connecting point is the Z-RIB, which appears to extend slightly into the I band. A difficulty with this suggestion is that this relaxed interconnecting body is not visible in cross sections of the Z band in the bw form or in the reconstruction of the fish muscle Z band (Luther, 1991). Hence, the elastic filament to Z-RIB–binding site would have to migrate in the ss to bw transition. Alternately, the elastic filaments might bind to the axial filament near the I–Z junction. Such an attachment could account for the observed decrease in diameter of the axial filaments as they enter the Z band.

The observation of up to four cross connections joining to the axial filament within 5 nm is consistent with observations from electron micrographs of cross sections. Such observations reveal from zero to four cross-connecting filaments joining to each axial filament in projection images (Ullrick et al., 1977; Goldstein et al., 1982; Yamaguchi et al., 1985). However, the F-actin core of the axial filament presents at most two actin monomers in this short distance. A recent 3-D reconstruction of the α-actinin head bound to F-actin shows the head region binding to two nearby G-actin monomers on filamentous actin (McGough et al., 1994). Filamentous actin presents only two (nearly diametrically opposed) binding sites in ~3 nm. Binding sites related by an ~90 degree rotation about the filament axis occur every 6–7 subunits or 16–19 nm. If the cross-connecting Z-filaments are in fact α-actinin, it becomes difficult to account for our observation of as many as four orthogonal cross connections in a 5-nm axial distance. However, it should be noted that (*a*) the symmetry of the Z band is not likely to be determined solely by that of the F-actin–α-actinin binding sites since the symmetry and arrangement of the Z band is different in insect flight muscle (Ashhurst, 1967; Cheng and Deatherage, 1989), in fish white muscle (Luther, 1991), and in the present reconstruction. All three of these Z bands have axial filaments composed primarily of actin and cross-connecting filaments whose major component is thought to be α-actinin. (*b*) Enzymatic digestion experiments with calpain have shown that the actin–α-actinin interaction in vitro is different than that in the vertebrate Z band (Goll et al., 1991). This suggests that one of the other Z band proteins may influence the interaction (Vigoreaux, 1994), so that the structure of the Z band is not determined only by the F-actin–α-actinin interaction. (*c*) In some cases, α-actinin is observed to lie along the axial filament (Zimmer and Goldstein, 1987*b*; Luther, 1991). Thus, the apparent connecting point between a cross-connecting Z-filament and an axial filament may not be a strict indication of an actin–α-actinin binding site.

Conclusion

We have shown that the unstimulated rat soleus muscle Z band may be modeled as a set of interdigitating axial filaments interconnected in a pseudo-fourfold array. Cross-connecting Z-filaments bind to axial filaments from opposite sarcomeres by way of a relaxed interconnecting body (Z-RIB). The Z-RIB is parallel to the axial filaments and ends near the I–Z junction. We have also observed that from one to four cross-connecting Z-filaments may join the axial filament in a 5-nm stretch. Thus, the Z band can not reflect simply the symmetry of the F-actin core of the axial filament. Furthermore, we observe a longitudinal offset of axial filament attachment points, so that the cross-connecting filaments lie in a plane not strictly perpendicular to the axial filaments. This suggests that the axial filaments are not in longitudinal register inside the Z band. Interestingly enough, our reconstructions show a set of cross connecting filaments joining axial filaments from the same sarcomere in the I band near to the Z. The distances between connecting points for these cross connections show a distribution similar to that observed in the Z band.

Our Z band reconstructions also reveal that all axial filaments do not traverse the complete Z band. Some are observed to terminate before seeking the opposite I–Z junction. It is possible that the disorder seen in our reconstructions reflects a physiological state of the muscle in which the Z band has not completely made the transition to the ss lattice.

It is difficult, however, to reconcile easily our reconstructed motif with the structural transitions previously observed in rat soleus muscle. When fixed with the muscle in tetanus, the Z band is seen to exhibit the bw pattern in cross section, with an enlargement of the Z spacing to ~24 nm (Goldstein et al., 1986). In this lattice form, there is no evidence in projection for a region of protein density halfway between the axial filaments. The cross-connecting Z-filaments appear to connect axial filaments from opposite sarcomeres in cross-sectional projections of this bw lattice. Thus, a ss to bw transition seems to require the elimination of the Z-RIB.

It is possible that the cross-connecting Z-filaments do not attach directly between axial filaments from the same sarcomere, but follow a bending path by binding to an axial filament, binding to or lying along another cross-connecting Z-filament, and then binding to an axial filament from the opposing sarcomere as illustrated in Fig. 8 *a*. In this case, the cross-connecting Z-filaments would separate along the length of the Z-RIB during the transition. The distance traversed between the axial filament attachment points becomes 17–30 nm in the bw lattice, so that the cross-connecting Z-filament would have to wrap around or lie along each axial filament for a distance of 5–12 nm after the transition. Alternately, cross-connecting Z-filaments could connect directly between axial filaments from the same sarcomere, with the Z-RIB providing an indirect attachment between the opposite sarcomeres. Then, the ss–bw transition would require a rearrangement in which the Z-RIB would be eliminated and cross-connecting filaments would be released to seek binding sites on axial filaments from opposing sarcomeres. It is apparent in either case that the structural change required for the transition implies a dynamic role for the Z band during contraction.

The authors thank R.J. Edwards for aid with electron microscopy and many illuminating discussions, and Professor James K. Stoops for the use of his computer facilities. Initial electron microscopy was done by the late David Murphy.

This research was partially supported by National Institutes of Health grant HL17376.

Received for publication 19 December 1995 and in revised form 5 February 1996.

References

Ashhurst, D.E. 1967. Z-line of the flight muscle of belostomid water bugs. *J. Mol. Biol.* 27:385–389.

Auber, J., and R. Couteaux. 1963. Ultrastructure de la strie Z dans des muscles de diteres. *J. Microsc. (Paris).* 2:309–324.

Bretaudiere, J.-P., J. Tapon-Bretaudiere, and J.K. Stoops. 1988. Structure of native alpha-2-macroglobulin and its transformation to the protease bound form. *Proc. Natl. Acad. Sci. USA.* 85:1437–1441.

Cheng, N., and J.F. Deatherage. 1989. Three-dimensional reconstruction of the Z disk of sectioned bee flight muscle. *J. Cell Biol.* 108:1761–1774.

Crowther, R.A., D.J. DeRosier, and A. Klug. 1970. The reconstruction of a three-dimensional structure from projections and its application to electron microscopy. *Proc. R. Soc. Lond. A.* 317:319–340.

Davey, D.F. 1976. The relation between Z-disk lattice spacing and sarcomere length in sartorius muscle fibers from *Hyla cerula. Australian Journal of Experimental Biology and Medical Science.* 54:441–447.

Deatherage, J.F., N. Cheng, and B. Bullard. 1989. Arrangement of filaments and cross-links in the bee flight muscle Z disk by image analysis of oblique sections. *J. Cell Biol.* 108:1775–1782.

Elliott, G.F., J. Lowy, and B.M. Millman. 1967. Low angle x-ray diffraction studies of living striated muscle during contraction. *J. Mol. Biol.* 25:31–45.

Fardeau, M. 1969. Ultrastructure des fibres musculaires squelettiques (I). *La Presse Medicale.* 77:1341–1344.

Frank, J., A. Verschoor, and M. Boublik. 1981. Computer averaging of electron micrographs of 40S ribosomal subunits. *Science (Wash. DC).* 214:1353–1355.

Frank, J., and M. Radermacher. 1986. *In* Advanced Techniques in Biological Electron Microscopy. J. Kohler, editor. Springer-Verlag, Berlin. 1–72.

Franzini-Armstrong, C. 1973. The structure of a simple Z line. *J. Cell Biol.* 58: 630–642.

Fürst, D.O., M. Osborn, R. Nave, and K. Weber. 1988. The organization of titin filaments in the half-sarcomere revealed by monoclonal antibodies in immunoelectron microscopy: a map of ten nonrepetitive epitopes starting at the Z line extends close to the M line. *J. Cell Biol.* 106:1563–1572.

Goldstein, M.A., J.P. Schroeter, and R.L. Sass. 1977. Optical diffraction of the Z lattice in canine cardiac muscle. *J. Cell Biol.* 79:818–836.

Goldstein, M.A., M.H. Stromer, J.P. Schroeter, and R.L. Sass. 1980. Optical reconstruction of nemaline rods. *Exp. Neurol.* 70:83–97.

Goldstein, M.A., J.P. Schroeter, and R.L. Sass. 1982. The Z-band in a slow skeletal muscle. *J. Muscle Res. Cell Motil.* 3:333–348.

Goldstein, M.A., L.H. Michael, J.P. Schroeter, and R.L. Sass. 1986. The Z-band lattice in skeletal muscle before, during, and after tetanic contraction. *J. Muscle Res. Cell Motil.* 7:527–536.

Goldstein, M.A., L.H. Michael, J.P. Schroeter, and R.L. Sass. 1987. Z band dynamics as a function of sarcomere length and the contractile state of muscle. *FASEB (Fed. Am. Soc. Exp. Biol.) J.* 1:133–142.

Goldstein, M.A., J.P. Schroeter, and R.L. Sass. 1990. Two structural states of the vertebrate Z band. *Electron Microsc. Rev.* 3:227–248.

Goll, D.E., W.R. Dayton, I. Singh, and R.M. Robson. 1991. Studies of the alpha-actinin/actin interaction in the Z-disk by using calpain. *J. Biol. Chem.* 266:8501–8510.

Harford, J., P. Luther, and J. Squire. 1994. Equatorial A-band and I-band x-ray diffraction from relaxed and active fish muscle. *J. Mol. Biol.* 239:500–512.

Hawkes, P.W. 1992. The electron microscope as a structure projector. *In* Electron Tomography. J. Frank, editor. Plenum Press. New York. 17–38.

Hessler, D., S.J. Young, B. Carragher, M. Martone, J. Hinshaw, R. Milligan, E. Masliah, M. Whittaker, S. Lamont, and M. Ellisman. 1992. SYNU: software for visualization of 3-dimensional biological structures. *In* Microscopy: the Key Research Tool. C.E. Lyman, L.D. Peachey, and R.M. Fisher, editors. EMSA, Milwaukee, WI. 73–82.

Holmes, K.C., D. Popp, W. Gebhard, and W. Kabsch. 1990. Atomic model of the actin filament. *Nature (Lond.).* 347:44–49.

Hoppe, W., and R. Hegerl. 1980. Three-dimensional structure determination by electron microscopy (non-periodic objects). *Top. Curr. Physics.* 13:144–185.

Huxley, H.E., and W. Brown. 1967. The low-angle x-ray diagram of vertebrate striated muscle and its behaviour during contraction and rigor. *J. Mol. Biol.* 30:383–434.

Irving, T.C., and B.M. Millman. 1992. Z-line/I-band and A-band lattices of intact frog sartorius muscle at altered interfilament spacing. *J. Muscle Res. Cell Motil.* 13:100–105.

Kelly, D.E. 1967. Models of muscle Z-band fine structure based on a looping filament configuration. *J. Cell Biol.* 34:827–840.

Kelly, D.E., and M.A. Cahill. 1972. Filamentous and matrix components of skeletal muscle Z-disks. *Anat. Rec.* 172:623–642.

Knappeis, G.G., and F. Carlsen. 1962. The ultrastructure of the Z disk in skeletal muscle. *J. Cell Biol.* 13:323–335.

Landon, D.N. 1970. The influence of fixation upon the fine structure of the Z disc of rat striated muscle. *J. Cell Sci.* 6:257–276.

Lawrence, M.C. 1992. Least squares method of alignment using markers. *In* Electron Tomography. J. Frank, editor. Plenum Press, New York. 197–204.

Luther, P.K. 1991. Three-dimensional reconstruction of a simple Z-band in fish muscle. *J. Cell Biol.* 113:1043–1055.

McGough, A., M. Way, and D. DeRosier. 1994. Determination of the α-actinin-binding site on actin filaments by cryoelectron microscopy and image analysis. *J. Cell Biol.* 126:433–443.

Morris, E.P., G. Nneji, and J.M. Squire. 1990. The three-dimensional structure of the nemaline rod Z-band. *J. Cell Biol.* 111:2961–2978.

Penczek, P.A., R.A. Grassucci, and J. Frank. 1994. The ribosome at improved resolution: new techniques for merging and orientation refinement in 3-D cryo-electron microscopy of biological particles. *Ultramicroscopy.* 53:251–270.

Podlubnaya, Z.A., L.A. Tskhovrebove, M.M. Zaalishivilli, and G.A. Stefanenko. 1975. Electron microscopic study of alpha-actinin. *J. Mol. Biol.* 95: 85–90.

Radermacher, M., T. Wagenknecht, A. Verschoor, and J. Frank. 1987. Three-dimensional reconstruction from a single-exposure, random conical tilt series applied to the 50S ribosomal subunit of *Escherichia coli. J. Microsc. (Oxf.).* 146:113–136.

Radermacher, M. 1988. Three-dimensional reconstruction of single particles from random and non-random tilt series. *Journal of Electron Microscopy Technique.* 9:359–394.

Radermacher, M. 1992. Weighted back-projection methods. *In* Electron Tomography. J. Frank, editor. Plenum Press, New York. 91–115.

Reedy, M.K. 1964. The structure of actin filaments and the origin of the axial periodicity in the I substance of vertebrate striated muscle. *Proc. R. Soc. Lond. B Biol. Sci.* 160:458–460.

Reedy, M.K., J.D. Etlinger, M. Rabinowitz, D.A. Fischman, and R. Zak. 1975. Removal of Z-lines and alpha-actinin from isolated myofibrils by a calcium-activated neutral protease. *J. Biol. Chem.* 250:4278–4284.

Rowe, R.W.D. 1973. The ultrastructure of the Z discs from white, intermediate, and red fibers of mammalian striated muscles. *J. Cell Biol.* 57:261–277.

Schroeter, J.P., J.-P. Bretaudiere, and M.A. Goldstein. 1991. Similar features in Z bands of both skeletal and cardiac muscle revealed by image enhancement. *Journal of Electron Microscopy Technique.* 19:296–304.

Schroeter, J.P., and J.-P. Bretaudiere. 1996. SUPRIM: easily modified image processing software. *J. Struct. Biol.* 116:131–137.

Suzuki, A.D., E. Boll, I. Singh, R.E. Allen, R.M. Robson, and M.H. Stromer. 1976. Some properties of purified skeletal muscle alpha-actinin. *J. Biol. Chem.* 251:6860–6870.

Takahashi, K., and A. Hattori. 1989. Alpha-actinin is a component of the Z-filament, a structural backbone of skeletal muscle Z-disks. *J. Biochem.* 105:529–536.

Tidball, J.G., G. Salem, and R. Zernicke. 1993. Site and mechanical conditions for failure of skeletal muscle in experimental strain injuries. *J. Appl. Physiol.* 74:1280–1286.

Tokuyasu, K.T., A.H. Sutton, B. Geiger, and S.J. Singer. 1981. Ultrastructure of chicken cardiac muscle as studied by double immunolabeling in electron microscope. *Proc. Natl. Acad. Sci. USA.* 78:7619–7623.

Trombitas, K., P.H.W.W. Baatsen, and G.H. Pollack. 1988. I-bands of striated muscle contain lateral struts. *J. Ultrastruct. Mol. Struct. Res.* 100:13–30.

Tskhovrebova, L.A. 1991. Vertebrate muscle Z-line structure: an electron microscopic study of negatively-stained myofibrils. *J. Musc. Res. Cell Motil.* 12: 425–438.

Ullrick, W.C., P.A. Toselli, J.D. Saide, and W.P.C. Phear. 1977. Fine structure of the vertebrate z-disc. *J. Mol. Biol.* 115:61–74.

Vigoreaux, J.O. 1994. The muscle Z band: lessons in stress management. *J. Muscle Res. Cell Motil.* 15:256–266.

Wang, K., and R. Ramirez-Mitchell. 1983. A network of transverse and longitudinal intermediate filaments is associated with sarcomeres of adult vertebrate skeletal muscle. *J. Cell Biol.* 96:562–570.

Yamaguchi, M., R.M. Robson, and M.H. Stromer. 1983*a*. Evidence for actin involvement in cardiac Z-lines and Z-line analogues. *J. Cell Biol.* 96:435–442.

Yamaguchi, M., R.M. Robson, M.H. Stromer, N.R. Cholvin, and M. Izumimoto. 1983*b*. Properties of soleus muscle Z-lines and induced Z-line analogs revealed by dissection with Ca^{2+}-activated neutral protease. *Anat. Rec.* 206: 345–362.

Yamaguchi, M., M. Izumimoto, R.M. Robson, and M.H. Stromer. 1985. Fine structure of wide and narrow vertebrate muscle Z lines. *J. Mol. Biol.* 184: 621–644.

Yu, L.C., R.W. Lymn, and R.J. Podolsky. 1977. Characterization of a non-indexable equatorial x-ray reflection from frog sartorius muscle. *J. Mol. Biol.* 115:455–464.

Zimmer, D.B., and M.A. Goldstein. 1987*a*. DNAse I interactions with filaments of skeletal muscles. *J. Muscle Res. Cell Motil.* 8:30–38.

Zimmer, D.B., and M.A. Goldstein. 1987*b*. Immunolocalization of alpha-actinin in adult chicken skeletal muscles. *Journal of Electron Microscopy Technique.* 6:357–366.